12th International Symposium on Turbulence and Shear Flow Phenomena (TSFP12)
Osaka, Japan, July 19–22, 2022

EFFECT OF STREAMWISE DOMAIN SIZE ON THE POD MODE CHARACTERISTICS IN AN ADVERSE PRESSURE GRADIENT TURBULENT BOUNDARY LAYER

Muhammad Shehzad, Bihai Sun, Daniel Jovic, Callum Atkinson, Julio Soria
Laboratory for Turbulence Research in Aerospace & Combustion (LTRAC),
Department of Mechanical and Aerospace Engineering
Monash University
Clayton, 3800, Victoria, Australia
Muhammad.shehzad@monash.edu, Bihai.Sun@monash.edu, Daniel.Jovic@monash.edu

Yasar Ostovan, Christophe Cuvier, Jean-Marc Foucaut
Univ. Lille, CNRS, ONERA, Arts et Metiers Institute of Technology, Centrale Lille, UMR 9014
Laboratoire de Mécanique des Fluides de Lille (LMFL) - Kampé de Fériet
Lille, F-59000, France
yasar.ostovan@centralelille.fr, christophe.cuvier@centralelille.fr, jean-marc.foucaut@centralelille.fr

Christian Willert
Institute of Propulsion Technology
German Aerospace Center (DLR)
Cologne, Germany
chris.willert@dlr.de

ABSTRACT

Proper orthogonal decomposition (POD) is used to study coherent structures on measurements of wall-bounded turbulent flows. In order to apply POD in the study of turbulent boundary layers, it is important to determine the appropriate size of the flow domain to be used in POD analysis. This study uses the 2C-2D PIV measurements of an adverse pressure gradient (APG) turbulent boundary layer (TBL) with $\beta \approx 0 \sim 3.74$ and $Re_{\delta_2} \approx 1,720 \sim 23,430$ where Re_{δ_2} is the momentum thickness based Reynolds number and β is the Clauser's pressure gradient parameter. The measurements were obtained in the Laboratoire de Mécanique des Fluides de Lille (LMFL) High-Reynolds-Number (HRN) Boundary Layer Wind Tunnel, Lille, France. Spanning over 20δ along the streamwise direction (where δ is the boundary layer thickness in the middle of the field of view), these are appropriate to be used in the study of the extent of the large-scale motions. POD analysis on the variable domain size along the streamwise direction (Δx) suggests that the POD mode shape changes with Δx. In this particular TBL, the shape of the first mode which represents the largest scales in the fluid flow, changes until Δx is equal to or greater than 8δ. It is also observed the smaller scales of higher-order POD modes take longer Δx to converge in the mode shape. The streamwise integral-length-scale of 6.68δ also confirms the size of the largest scales to be around 8δ. Therefore, for this particular TBL, a minimum streamwise domain size of 8δ is appropriate for the analysis of large-scale motions using POD.

1 Introduction

POD has been used as a tool to study the coherent structures including large-scale motions (LSMs) since its first application in fluid dynamics by Lumley (1967). It is a generalization of the conventionally used Fourier power spectral analysis and is used to investigate the TKE distribution as a function of scale in a TBL flow that is inhomogeneous in the streamwise direction (Liu *et al.*, 2001). POD has been used by Lengani *et al.* (2017) to highlight the lift-up mechanism as well as the instability of the low-speed streaks that initiate the transition in a boundary layer under a strong APG. Bakewell Jr & Lumley (1967) used POD to study the randomly distributed counter-rotating eddies as LSMs in a turbulent pipe flow at a $Re_D = U_b D/\nu = 8,700$, where U_b is the bulk velocity and D is the pipe diameter. Liu *et al.* (2001) used POD to evaluate the scales contributing toward the events that produce TKE and Reynolds shear stress from 2D data of channel flows at $Re_h = U_b h/\nu = 5,378$ and $29,935$ (where h represents the channel half-height) and concluded that the LSMs contain a large fraction of the Reynolds streamwise stress and a small fraction of Reynolds wall-normal stress. Wu (2014) studied the intense LSMs in a ZPG-TBL at $Re_{\delta_2} = 8200$ and 12000 and performed POD to establish a connection between the first two dominant POD modes and the instantaneous large-scale structures. This study concluded that the Reynolds streamwise stress, Reynolds shear stress and the spatial velocity correlation functions are reduced without the intense LSMs and deduced that the LSMs are significant contributors to the most energetic POD mode which is the first mode.

In this paper, a brief description of proper orthogonal decomposition is presented, which is followed by its application to the streamwise and wall-normal velocity fluctuations of a turbulent boundary layer obtained using 2C-2D PIV. The effect of the streamwise and wall-normal domain size on the properties of POD modes is investigated.

Throughout this paper, the x, y and z are taken as the streamwise, wall-normal and spanwise directions, respectively. The instantaneous, mean and fluctuating velocities in the x direction are referred to as u, U and u', respectively. Accordingly, the velocities in the y direction are represented by v.

2 Proper orthogonal decomposition (POD)

In this study, the snapshot-POD, which was introduced by Sirovich (1987), is used to extract modes based on optimizing the mean square of the fluctuating velocity. A brief description of the POD method is as follows:

Consider a set of fluctuating velocity fields $\overline{\overline{\boldsymbol{u'}}}(x,y,t)$ given by

$$\overline{\overline{\boldsymbol{u'}}}(x,y,t) = [\boldsymbol{u'}(x,y,t_1) \;\; \boldsymbol{u'}(x,y,t_2) \;\; ... \;\; \boldsymbol{u'}(x,y,t_N)] \in \mathbb{R}^{M\times N}, \quad M \gg N, \tag{1}$$

where N is the number of snapshots, *i.e.* the velocity fields, and M is the number of data points in each snapshot, which is equal to the number of velocity components multiplied by the number of grid points, and

$$\boldsymbol{u'}(x,y,t) = \begin{bmatrix} u'(x,y,t) \\ v'(x,y,t) \end{bmatrix}.$$

$\overline{\overline{\boldsymbol{u'}}}(x,y,t)$ can be written as

$$\overline{\overline{\boldsymbol{u'}}}(x,y,t) = \sum_{i=1}^{N} \psi_i(t)\phi_i(x,y), \tag{2}$$

where $\phi_i(x,y)$ is the ith spatial mode and $\psi_i(t)$ is the set of the corresponding temporal coefficients. Defining the covariance matrix $\boldsymbol{R}$ of the vector $\boldsymbol{u'}(x,y,t)$ as

$$\boldsymbol{R} = \boldsymbol{X}\boldsymbol{X}^T, \;\; \boldsymbol{R} \in \mathbb{R}^{M\times M} \tag{3}$$

with $\boldsymbol{X} = \overline{\overline{\boldsymbol{u'}}}$, the classical POD of Lumley (1967) yields

$$\boldsymbol{R}\phi_i = \lambda_i\phi_i, \;\; \phi_i \in \mathbb{R}^M, \tag{4}$$

where $i = 1, 2, \ldots, M$ and λ_i represents the eigenvalue of the i^{th} POD mode. In the snapshot-POD method, the matrix $\boldsymbol{X}^T\boldsymbol{X}$ is used instead of $\boldsymbol{X}\boldsymbol{X}^T$, which is much smaller in size but yields the same nonzero eigenvalues (Sirovich, 1987). Hence, we can write

$$\boldsymbol{X}^T\boldsymbol{X}\psi_i = \lambda_i\psi_i, \;\; \psi_i \in \mathbb{R}^N. \tag{5}$$

The corresponding spatial mode ϕ_i can be computed as

$$\phi_i = \boldsymbol{X}\psi_i\frac{1}{\sqrt{\lambda_i}}. \tag{6}$$

This can also be written as

$$\boldsymbol{\Phi} = \boldsymbol{X}\boldsymbol{\Psi}\boldsymbol{\Lambda}^{-1/2}, \tag{7}$$

where the columns of $\boldsymbol{\Phi}$ are the vectors of the spatial modes ($\boldsymbol{\Phi} = \begin{bmatrix}\phi_1 \; \phi_2 \; ... \; \phi_N\end{bmatrix} \in \mathbb{R}^{M\times N}$), the columns of $\boldsymbol{\Psi}$ are the vectors of temporal coefficients corresponding to each POD mode ($\boldsymbol{\Psi} = \begin{bmatrix}\psi_1 \; \psi_2 \; ... \; \psi_N\end{bmatrix} \in \mathbb{R}^{N\times N}$) and $\boldsymbol{\Lambda}$ is the vector of eigenvalues corresponding to each POD mode ($\boldsymbol{\Lambda} = \begin{bmatrix}\lambda_1 \; \lambda_2 \; ... \; \lambda_N\end{bmatrix} \in \mathbb{R}^N$).

The TKE of the boundary layer flow equals to half of the sum of the eigenvalues, *i.e.*

$$k = \frac{1}{2}\overline{\boldsymbol{u'^2}} = \frac{1}{2}\sum_{i=1}^{N}\lambda_i\,. \tag{8}$$

3 Experimental method

This study uses the 2C-2D PIV measurements of an APG-TBL that were taken in the $x-y$ plane in the LMFL HRN wind tunnel. This facility has a 2-m wide, 1-m high and 20.6-m long test section. A schematic diagram of the LMFL wind tunnel is shown in figure 1 with three sections that have different pressure conditions: zero pressure gradient (ZPG), favourable pressure gradient (FPG) and APG. The APG-TBL measurements cover about 21δ in the streamwise direction and from 0.02δ to 1.45δ in the wall-normal direction. These measurements were obtained using 16 sCMOS cameras in a 3.466 m long continuous field of view (FOV) and were used in the characterization of a high-Reynolds-number APG-TBL developing over the considerably long regions (Cuvier *et al.*, 2017). The FOVs of the LFOV measurements are also highlighted in figure 1. Since the measurements of the current APG-TBL were originally presented by Cuvier *et al.* (2017), the reader is referred to that paper for the complete experimental details.

To compare the first- and second-order statistics of the current APG-TBL with a ZPG-TBL, the 2C-2D PIV measurements of the latter taken in the $x-y$ plane of the same experimental facility are also included. The ZPG-TBL measurements cover about 2.61δ in the streamwise direction, and from 0.02δ to 3.12δ in the wall-normal direction. The experimental and PIV analysis parameters of the current APG-TBL are presented in table 1.

The current measurements of both TBLs do not cover the region from the wall to the end of the buffer layer. Therefore, the inner-layer measurements of two TBLs obtained in the same location of the same facility as the current TBLs, have also been included in the comparison of the first and second-order statistics. These inner-layer measurements have a higher spatial resolution (HSR) in the wall-normal direction and were taken at a time different to the outer-layer measurements. The HSR measurements of the ZPG-TBL and the APG-TBL, when compared to outer-layer measurements, are approximately 5 times more spatially resolved in the streamwise direction and more than 14 times in the wall-normal direction, respectively.

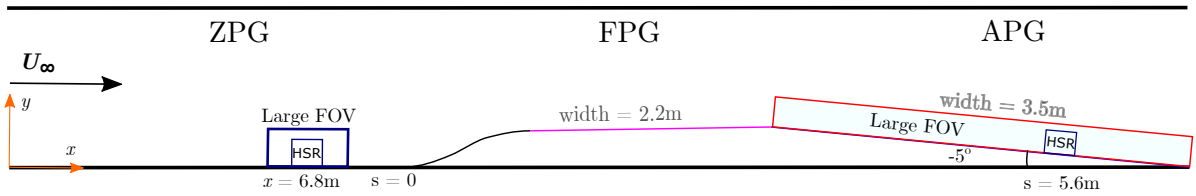

Figure 1. Schematic of the test section in the LML Wind Tunnel. Figure adapted from Cuvier *et al.* (2017).

Table 1. PIV analysis parameters. Source for the outer-layer measurements of the APG-TBL: Cuvier *et al.* (2017).

Measurement	ZPG-TBL	APG-TBL
Inflow Velocity (m/s)	9	9
Viscous length scale l^+ (μm)	42	44
FOV ($l^+ \times l^+$)	$6,342 \times 7,218$	$78,847 \times 5,801$
(pixels × pixels)	$2,338 \times 2,786$	$32,494 \times 2,391$
(mm × mm)	266×317	$3,466 \times 254$
Grid spacing ($l^+ \times l^+$)	25×25	24×24
(pixels × pixels)	7×7	10×10
IW size ($l^+ \times l^+$)	57×57	58×58
(pixels × pixels)	16×16	24×24
Frequency (Hz)	5	4
Number of samples	10,000	30,000
Vector field size	334×398	$3,250 \times 238$

For the complete experimental details of the inner-layer (HSR) measurements, the reader is referred to Shehzad *et al.* (2021).

The boundary layer parameters for both TBLs are adopted from Cuvier *et al.* (2017) and presented in table 2.

Table 2. The boundary layer parameters at the middle of the FOVs of the ZPG- and APG-TBLs.

	ZPG-TBL	APG-TBL
Edge velocity, U_e (m/s)	9.64	11.90
Boundary layer thickness, δ (mm)	102	165
Displacement thickness, δ_1 (mm)	16.4	26.9
Momentum thickness, δ_2 (mm)	12.0	18.75
Shape factor, H	1.37	1.43
Momentum thickness based Reynolds number, Re_{δ_2}	7,750	14,830
Clauser's pressure gradient parameter, β	-	2.11

4 First- and second-order statistics

The mean velocity profiles of both TBLs scaled with the outer variables δ_1 and U_e are shown in figure 2(a). Likewise, the Reynolds stress profiles are also scaled with outer variables and shown in figure 2(b). As it is clear from these figures, the outer-layer measurements are consistent with the inner-layer HSR measurements. The ZPG-TBL has one inner peak in Reynolds streamwise stresses and no outer peak. The APG-TBL has an outer peak located around $y = 1.3\delta_1$ that is as strong as the inner peak. The Reynolds wall-normal and shear stresses in the outer region have outer peaks in the APG-TBL and plateaus in the ZPG-TBL.

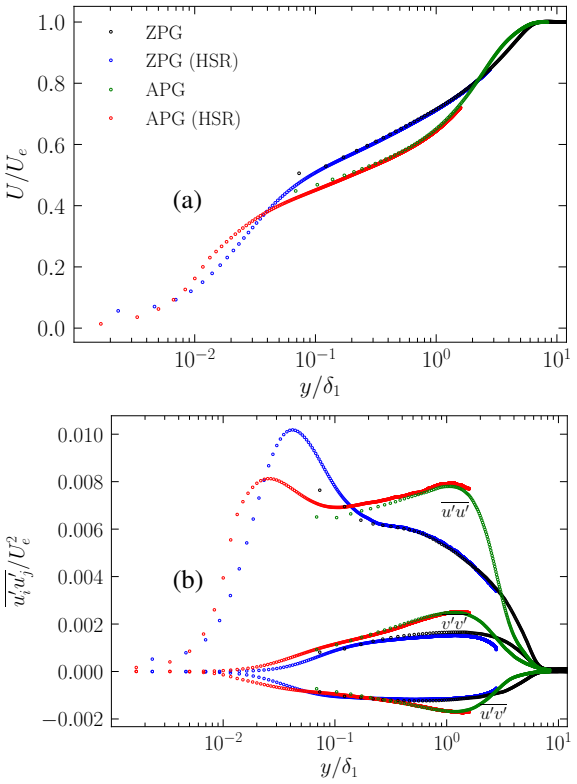

Figure 2. The outer-scaled profiles of the (a) mean streamwise velocity and (b) the Reynolds stresses.

5 Effect of streamwise domain size on POD modes

Among many of its applications, POD can be used to separate the snapshots carrying intense LSMs from an overall ensemble of snapshots. It can also be used to separate the large-scale motions from the small-scale motions based on a threshold value of the cumulative turbulent kinetic energy (CTKE). Before it is applied to a turbulent boundary layer dataset, it is worthwhile

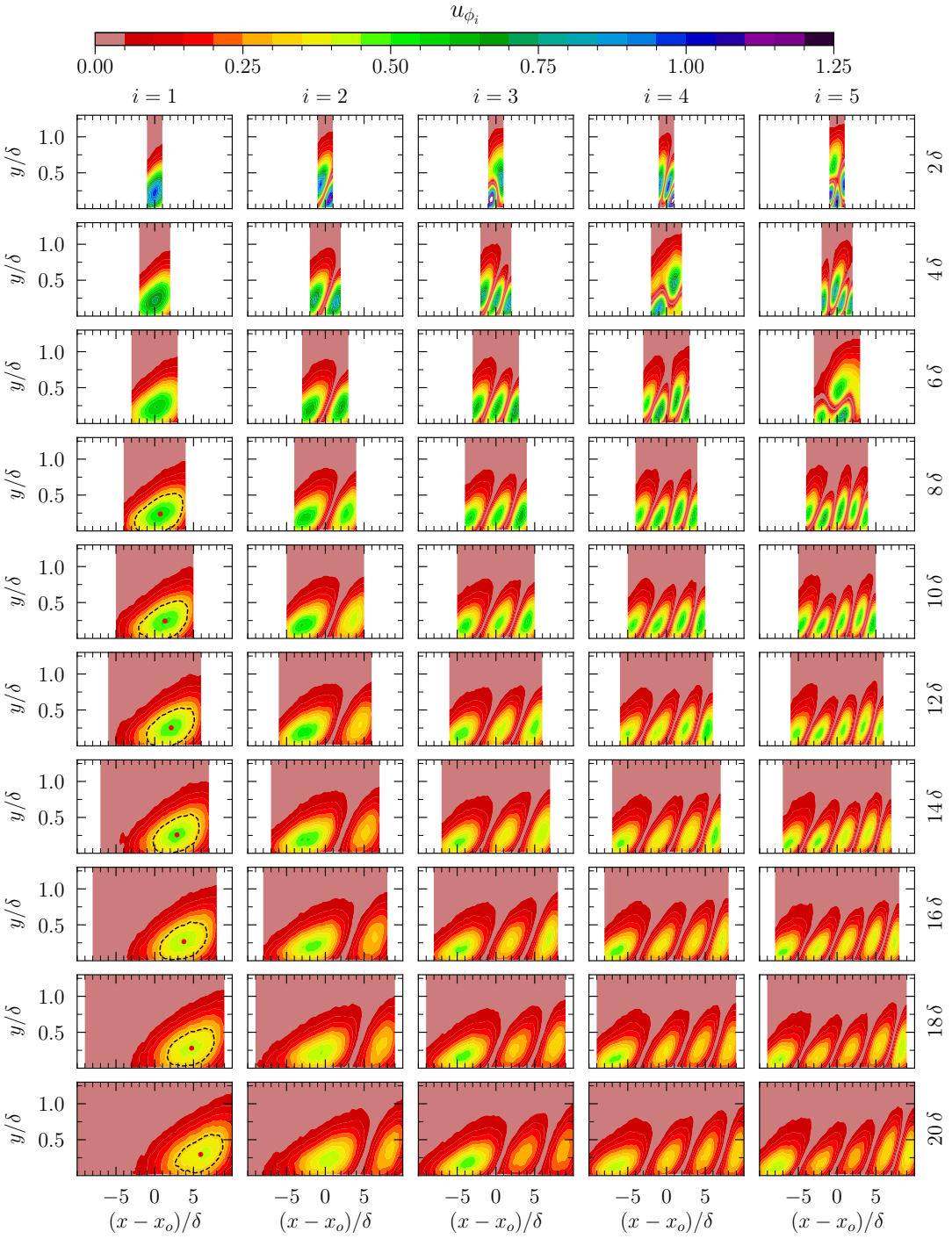

Figure 3. The contours of the first five POD modes as a function of Δx that varies from 2δ to 20δ with increments of 2δ. Each mode has been normalized with the peak value in the first mode for $\Delta x = 2\delta$. For $\Delta x \geq 8\delta$, the iso-contour at the correlation level of $C = 0.32$ is highlighted with a dashed black line and its centroid with a red dot.

to investigate the effect of the domain size of the velocity fluctuations data in the streamwise direction, on the properties of the POD modes and the result of any of its applications, for example, the conditional statistics of the intense large-scale motions.

To perform this analysis, one needs a dataset that has a sufficiently long streamwise range to contain the longest of the coherent structures reported in the previous studies. Hutchins & Marusic (2007) report that the large-scale structures are elongated in the streamwise direction with lengths of up to 20δ. Since the outer-layer measurements of the APG-TBL have Δx of about 21δ, these are suitable for this particular analysis. Since the large-scale motions are dominant in the outer region (Hambleton *et al.*, 2006), the wall-normal range of 0.02δ to 1.45δ of the APG-TBL measurements is also appropriate for this application.

Figure 3 shows the contours of the first five POD modes as a function of the streamwise domain size Δx which varies from 2δ to 20δ with increments of 2δ. These modes have been normalized with the maximum value of the first POD mode for $\Delta x = 2\delta$. The Δx of 2δ to 6δ do not cover the full mode shape in the first mode for the iso-contour levels C of 0.2 to

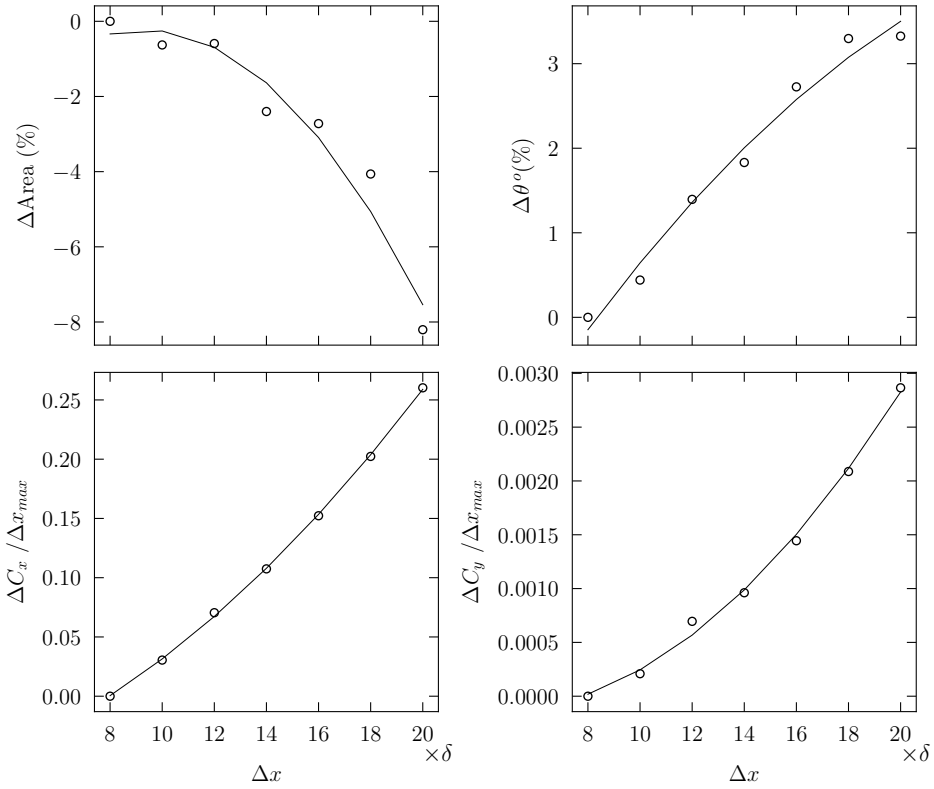

Figure 4. Properties of the iso-contour at $C = 0.32$ in the first POD mode as a function of Δx. The solid lines represent the quadratic curve fits.

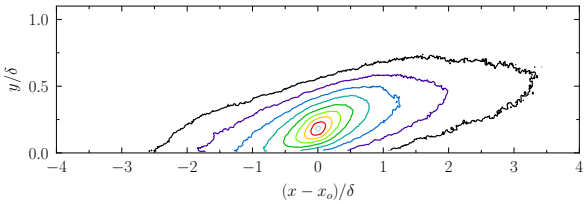

Figure 5. Two-point correlation of the streamwise velocity fluctuations ρ_{uu} at the streamwise middle of the large-field measurements of the APG-TBL. This streamwise location corresponds to $\beta = 2.01$. The iso-contour levels vary from 0.15 to 0.95 with increments of 0.1. In the wall-normal direction, the correlation is centred at $y = \delta_1$.

1.0. $\Delta x = 8\delta$ contains the whole structure for the iso-contour levels of 0.2 to 1.0, and any larger Δx does not change the mode shape but shifts it rightwards. For $\Delta x \geq 8\delta$, $C = 0.32$ is highlighted with a dashed black line and its centroid with a red dot. In this range, the mode shape does not change but the centroid of $C = 0.32$ is shifted rightwards with an increase in Δx.

The geometrical properties of the first POD mode as a function of Δx are presented in figure 4. When Δx increases from 8δ to 20δ, the area of $C = 0.32$ decreases quadratically by almost 8% whereas its inclination angle increases by approximately 3.5%. The x-coordinate of the centroid is shifted rightwards by approximately 25% of the maximum streamwise domain size (Δx_{max}) and the y-coordinate is shifted upwards by approximately 3% of Δx_{max}. The changes in the inclination angle and both coordinates of the centroid are weakly quadratic.

For the streamwise domain size of $\Delta x < 8\delta$, the shapes of all five POD modes are not converged. One can also observe that the higher the mode number, the longer Δx it takes to converge the mode shape. This means that the smaller scales of the higher mode numbers need a larger Δx to converge. For $\Delta x \geq 8\delta$, the shapes of the second to the fifth POD modes do not change much qualitatively but are expanded a little bit in the x direction as Δx increases. Hence, it can be assumed that the POD mode shapes have almost converged at $\Delta x = 8\delta$. A larger Δx would not change the scales size much but any conditional averaging of the turbulent statistics on the velocity fluctuations which are reconstructed using the POD modes or the conditional averaging based on the temporal coefficients of the first mode may be affected by the considerable rightwards shifting of the centroid of an iso-contour in the first POD mode.

The first POD modes represent the LSMs, which populate the outer region of the turbulent boundary layer (Vila *et al.*, 2017). Since the $\Delta x \geq 8\delta$ contain the whole structure for the first POD mode for the iso-contour levels of 0.2 to 1.0, $\Delta x = 8\delta$ is assumed to be an appropriate domain size for the subsequent POD analysis on the APG-TBL dataset. It also indicates that the size of the large-scale structures in the APG-TBL is up to 8δ. The two-point correlation of the streamwise velocity fluctuations ρ_{uu} calculates the extent to which the scales are correlated in the streamwise direction, which is representative of the streamwise size of the large-scale motions. ρ_{uu} is defined as

$$\rho_{uu} = \frac{\overline{u'(x,y)u'(x+\Delta x, y+\Delta y)}}{\sqrt{\overline{u'^2(x,y)u'^2(x+\Delta x, y+\Delta y)}}}. \tag{9}$$

Figure 5 shows iso-contours of the two-point correlation of the streamwise velocity fluctuations, centred at the middle of the x domain and $y = \delta_1$. The integral-length-scale $l_{uu} = \int_{-\infty}^{\infty} \rho_{uu}\, dx$ is calculated to be 6.68δ. This further validates the argument that the size of large-scale motions in the current APG-TBL is up to 8δ. This is not consistent with the streamwise extent of LSMs reported by Hutchins & Marusic (2007) in a ZPG-TBL which is up to 20δ. Although the current TBL is under an APG, most of its properties are considerably close to the ZPG-TBL because of the low β values. Note that Hutchins & Marusic (2007) used Taylor's frozen hypothesis and a convection velocity based on the local mean velocity, on the single-point measurements of a hot-wire rake to reconstruct the velocity signal along the x axis, which may have affected the true indication of the length of the large-scale motions.

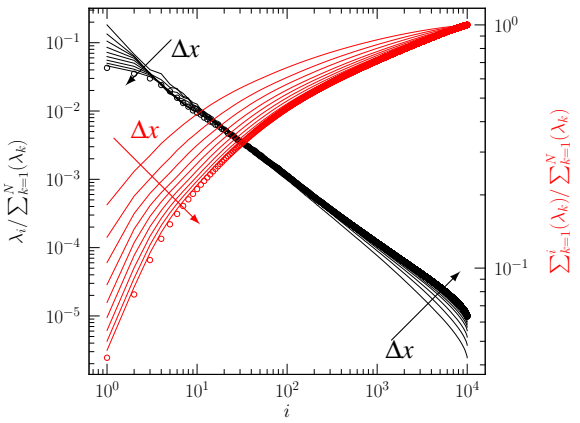

Figure 6. Effect of the streamwise domain size on POD eigenvalues. The domain size Δx is increasing from 8δ to 20δ in the directions of the arrows. The empty circles represent $\Delta x = 20\delta$ and the solid lines represent the other cases.

Figure 6 presents the relative contributions (black profiles) and the cumulative relative contributions (red profiles) of the POD modes to the total turbulent kinetic energy as a function of Δx. When Δx increases from 2δ to 20δ, the energy content of the first POD mode decreases from 18.22% to 4.28% and of the second mode from 6.77% to 3.51%. Oppositely, for the highest mode number, the energy content increases with an increase in Δx. The CTKE of the POD modes also decreases with an increase in Δx. This decrease is faster for the higher values of Δx and slower for the lower Δx. This shows that with an increase in Δx, the energy of the POD modes is shifted from the lower-order modes to the higher-order ones.

6 Conclusion

A change in the streamwise domain size of the measurements of a TBL affects the properties of its POD modes. For the particular case of the present APG-TBL, the shapes of the first five POD modes are not converged for a variable streamwise domain size until it is equal to or greater than 8δ. It is also observed that the smaller scales of higher-order POD modes take longer Δx to converge in the mode shape. For $\Delta x \geq 8\delta$, the area and the angle of an iso-contour at $C = 0.32$ in the first mode change only by approximately 8% and 3%, respectively, for a 2.5 times increase in Δx but its centroid is shifted rightwards by 25% of the maximum domain size. Hence, it is concluded that the size of the large-scale motions in this particular TBL is up to 8δ, which is also confirmed by its streamwise integral-length-scale of 6.68δ. It is also observed that an expanding flow domain shifts the energy contained in the lower-order POD modes to the higher-order modes. Based on this analysis, it is concluded and recommended that whenever and wherever possible, it is worthwhile to perform the POD analysis on variable streamwise domain size to find the appropriate size of the flow domain that covers the largest of the scales therein.

REFERENCES

Bakewell Jr, Henry P & Lumley, John L 1967 Viscous sublayer and adjacent wall region in turbulent pipe flow. *The Physics of Fluids* **10** (9), 1880–1889.

Cuvier, C, Srinath, S, Stanislas, M, Foucaut, JM, Laval, JP, Kähler, CJ, Hain, R, Scharnowski, S, Schröder, A, Geisler, R *et al.* 2017 Extensive characterisation of a high Reynolds number decelerating boundary layer using advanced optical metrology. *Journal of Turbulence* **18** (10), 929–972.

Hambleton, WT, Hutchins, N & Marusic, Ivan 2006 Simultaneous orthogonal-plane particle image velocimetry measurements in a turbulent boundary layer .

Hutchins, N & Marusic, Ivan 2007 Evidence of very long meandering features in the logarithmic region of turbulent boundary layers. *Journal of Fluid Mechanics* **579**, 1–28.

Lengani, Davide, Simoni, Daniele, Ubaldi, Marina, Zunino, Pietro & Bertini, Francesco 2017 Experimental study of free-stream turbulence induced transition in an adverse pressure gradient. *Experimental Thermal and Fluid Science* **84**, 18–27.

Liu, Z, Adrian, RJ & Hanratty, TJ 2001 Large-scale modes of turbulent channel flow: transport and structure. *Journal of Fluid Mechanics* **448**, 53.

Lumley, John Leask 1967 The structure of inhomogeneous turbulent flows. *Atmospheric turbulence and radio wave propagation* .

Shehzad, Muhammad, Sun, Bihai, Jovic, Daniel, Ostovan, Yasar, Cuvier, Christophe, Foucaut, Jean-Marc, Willert, Christian, Atkinson, Callum & Soria, Julio 2021 Investigation of large scale motions in zero and adverse pressure gradient turbulent boundary layers using high-spatial-resolution particle image velocimetry. *Experimental Thermal and Fluid Science* **129**, 110469.

Sirovich, Lawrence 1987 Turbulence and the dynamics of coherent structures. parts I-III. *Quarterly of applied mathematics* **XLV**, 561–590.

Vila, Carlos Sanmiguel, Örlü, Ramis, Vinuesa, Ricardo, Schlatter, Philipp, Ianiro, Andrea & Discetti, Stefano 2017 Adverse-pressure-gradient effects on turbulent boundary layers: statistics and flow-field organization. *Flow, turbulence and combustion* **99** (3), 589–612.

Wu, Yanhua 2014 A study of energetic large-scale structures in turbulent boundary layer. *Physics of Fluids* **26** (4), 045113.